Brain Image Analysis Using Spherical Splines

Ying He, Xin Li, Xianfeng Gu, and Hong Qin

Center for Visual Computing (CVC) and Department of Computer Science
Stony Brook University, Stony Brook, NY, 11794-4400, USA
{yhe, xinli, gu, qin}@cs.sunysb.edu

Abstract. We propose a novel technique based on spherical splines for brain surface representation and analysis. This research is strongly inspired by the fact that, for brain surfaces, it is both necessary and natural to employ spheres as their natural domains. We develop an automatic and efficient algorithm, which transforms a brain surface to a single spherical spline whose maximal error deviation from the original data is less than the user-specified tolerance. Compared to the discrete mesh-based representation, our spherical spline offers a concise (low storage requirement) digital form with high continuity (C^{n-1} continuity for a degree n spherical spline). Furthermore, this representation enables the accurate evaluation of differential properties, such as curvature, principal direction, and geodesic, without the need for any numerical approximations. Thus, certain shape analysis procedures, such as segmentation, gyri and sulci tracing, and 3D shape matching, can be carried out both robustly and accurately. We conduct several experiments in order to demonstrate the efficacy of our approach for the quantitative measurement and analysis of brain surfaces.

1 Introduction

The human cortical surface is a highly complex, folded structure with rich geometric, anatomical, and functional information. The outward folds (called gyri) and the cortical grooves (called sulci) encode important anatomical features which provide a parcellation of the cortex surface into anatomically distinct areas. Surface-based modeling is valuable in brain imaging to help analyze anatomical shape, to statistically combine or compare 3D anatomical models across subjects, and to map functional imaging parameters onto anatomical surfaces. Thus, various novel data analysis tools towards the quantitative study and better understanding of cortical surfaces have been developed in recent years. For example, Avants and Gee [1] develop a technique to estimate the shape operator and computes principal directions and curvatures. Cachia et al. present a mean curvature based primal sketch, which derived from a scale space computed for the mean curvature of the cortical surface [2]. Gu et al. study the conformal brain mapping [3] and present an algorithm for 3D shape matching using 2D conformal representations [4]. Tao et al. present a method for automatically finding curves of sulcal fundi on human cortical surfaces using statistical models [5, 6]. Thompson et al. present a technique for brain image warping in [7] and then apply it to detect disease-specific patterns in [8].

Recent developments in brain imaging have accelerated the collection of high-resolution data sets for cortical surfaces. Typically, the acquired digital models of cortical surfaces are in the form of triangular meshes. It is desirable and necessary to reverse-engineer a spline-based surface from meshes for many medical applications, leading to many advantages. For example, a continuous spline representation for a cortical surface facilitates the quantitative and accurate study of the anatomy of cortical surfaces, and consequently, provides a means for mapping functional activation sites over complicated geometry. In particular, we can precisely compute all the differential quantities such as geodesics, curvatures, and areas anywhere on cortical surfaces. In general, these local and global differential attributes will enable many medical imaging applications such as image segmentation/classification, tracking brain change in an individual over time, and surface quality analysis and control.

At present, tensor-product *B*-spline and NURBS are widely used for surface representation because of their many attractive geometric properties. Nevertheless, due to their rectangular structures, they are less suitable for the effective modeling and shape analysis of cortical surfaces. In contrast, because of the topological equivalence between spheres and brain surfaces, spherical splines appear to be more ideal for modeling brain surfaces, both in theory and in practice, than tensor product *B*-splines and NURBS. In this paper, we present a general framework to model brain surfaces with spherical triangular *B*-splines proposed by Pfeifle and Seidel [9]. These spline surfaces are defined on an arbitrary spherical triangulation and exhibit no degeneracies that frequently arise when attempting to employ planar parametric splines for modeling sphere-like, closed surfaces. Our specific contributions are as follows:

1. The shape is represented by a single degree n spline without any patching and stitching work. The maximal error deviation from the original data is less than any user-specified tolerance. The reconstructed surface is C^{n-1} continuous everywhere. The surface approximation procedure is automatic.
2. Based on its analytical representation, we can compute the differential properties, including normals, curvatures, geodesics, etc, without the need for any numerical approximations via frequently-used bilinear interpolation and/or local algebraic surface fitting. Therefore, the shape analysis procedures, such as segmentation, can be done robustly and accurately.
3. By analyzing the extrema of the derivative of principal curvatures with respect to the curvature directions, we can automatically detect the gyri and sulci curves to achieve quantitatively accurate results.
4. With the analytical formulation of conformal factor and mean curvature, we compare the 3D shapes using conformal representation robustly and accurately.

2 Surface approximation using spherical triangular *B*-splines

In this section, we briefly review the definition of spherical triangular *B*-splines and then introduce the algorithm for automatic conversion of the brain surface into a spherical triangular *B*-spline.

2.1 Spherical triangular *B*-spline

Denote by $\mathbb{S}^2 = \{\mathbf{x} | \mathbf{x} \in \mathbb{R}^3, \|\mathbf{x}\| = 1\}$ a unit sphere in $\mathbb{R}^3$. Let points $\mathbf{t}_i \in \mathbb{S}^2$, $i \in \mathbb{N}$, be given and define a spherical triangulation

$$T = \{\Delta(I) = [\mathbf{t}_{i_0}, \mathbf{t}_{i_1}, \mathbf{t}_{i_2}] : I = (i_0, i_1, i_2) \in \mathcal{I} \subset \mathbb{N}^3\},$$

where every triangle is oriented counter-clockwise (or clockwise). Next, with every vertex $\mathbf{t}_i$ of T we associate a cloud of knots $\mathbf{t}_{i,0}, \ldots, \mathbf{t}_{i,n}$ such that $\mathbf{t}_{i,0} = \mathbf{t}_i$. For every spherical triangle $I = [\mathbf{t}_{i_0}, \mathbf{t}_{i_1}, \mathbf{t}_{i_2}] \in T$,

1. all the triangles $X^I_\beta = [\mathbf{t}_{i_0,\beta_0}, \mathbf{t}_{i_1,\beta_1} \mathbf{t}_{i_2,\beta_2}]$ with $\beta = (\beta_0, \beta_1, \beta_2)$ and $|\beta| = \beta_0 + \beta_1 + \beta_2 \leq n$ are non-degenerate.
2. the set $\Omega^I_n = interior(\cap_{|\beta| \leq n} X^I_\beta)$ must be non-empty.

Then the spherical triangular *B*-spline basis function N^I_β, $|\beta| = n$, is defined by means of spherical simplex splines $M(\mathbf{u}|V^I_\beta)$ as $N(\mathbf{u}|V^I_\beta) = |\det(X^I_\beta)| M(\mathbf{u}|V^I_\beta)$ where $V^I_\beta = \{\mathbf{t}_{i_0,0}, \ldots, \mathbf{t}_{i_0,\beta_0}, \mathbf{t}_{i_1,0}, \ldots, \mathbf{t}_{i_1,\beta_1}, \mathbf{t}_{i_2,0}, \ldots, \mathbf{t}_{i_2,\beta_2}\}$.

A degree n spherical triangular *B*-spline surface $\mathbf{F}$ over T is then defined as

$$\mathbf{F}(\mathbf{u}) = \sum_{I \in T} \sum_{|\beta| = n} \mathbf{c}_{I,\beta} N(\mathbf{u}|V^I_\beta), \tag{1}$$

where $\mathbf{c}_{I,\beta} \in \mathbb{R}^3$ are the control points.

The spherical triangular *B*-spline has many useful properties, including:

– *Piecewise polynomial:* $\mathbf{F}(\mathbf{u})$ is a degree n piecewise polynomial defined on the sphere.
– *Locality:* The movement of a single control point $\mathbf{c}_{I,\beta}$ only influences the surface on the triangle I and on the triangles directly surrounding I.
– *Smoothness:* If the knots of each set V^I_β are in "spherical" general position (i.e., no three knots in V^I_β lie on the same great circle), then $\mathbf{F}(\mathbf{u})$ is C^{n-1} continuous everywhere.

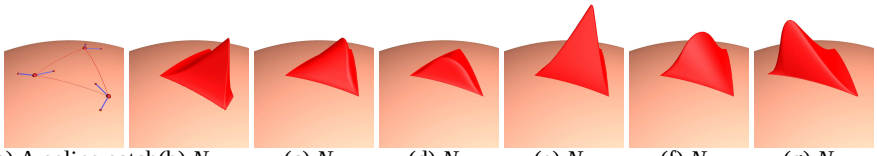

(a) A spline patch (b) N_{200} (c) N_{110} (d) N_{101} (e) N_{020} (f) N_{011} (g) N_{002}

Fig. 1. Six basis functions of a quadratic spherical spline patch.

Figure 1(a) shows a quadratic spherical spline patch defined on $\{\mathbf{t}_0, \mathbf{t}_1, \mathbf{t}_2\}$. We associate two sub-knots $\mathbf{t}_{i,j}$, $j = 1, 2$ with each vertex $\mathbf{t}_i$. The six basis functions are shown in Figure 1(b)-(g). Since no three knots are co-circular, every basis function is C^1 everywhere.

2.2 Surface reconstruction algorithm

The goal of surface reconstruction is to obtain a continuous representation of a surface described by a cloud of points or a mesh. The problem can typically be stated as follows: given a set $P = \{\mathbf{p}_i\}_{i=1}^m$ of points $\mathbf{p}_i \in \mathbb{R}^3$, find a smooth spherical spline $\mathbf{F} : \mathbb{S}^2 \to \mathbb{R}^3$ that approximates P.

A general framework for surface reconstruction is to minimize a linear combination of interpolation and fairness functionals, i.e.,

$$\min E = E_{dist} + \lambda E_{fair}. \tag{2}$$

The first part is

$$E_{dist} = \sum_{i=1}^{m} \|\mathbf{F}(\mathbf{u}_i) - \mathbf{p}_i\|^2$$

where $\mathbf{u}_i \in \mathbb{S}^2$ is parameter for $\mathbf{p}_i$, $i = 1, \ldots, m$. The second part E_{fair} in (2) is a smoothing term. A frequently used example is the thin plate energy, $E_{fair} = \iint_{\mathbb{S}^2} (\mathbf{F}_{uu}^2 + 2\mathbf{F}_{uv}^2 + \mathbf{F}_{vv}^2) dudv$. Both parts are quadratic functions of the unknown control points. For example, the approximation functional E_{dist} has the following form:

$$E_{dist} = \frac{1}{2}\mathbf{x}^T Q\mathbf{x} + \mathbf{c}^T\mathbf{x} + f,$$

where $\mathbf{x} = (\ldots, \mathbf{c}_{I,\beta}, \ldots)^T$,

$$Q = \begin{pmatrix} \vdots \\ \ldots\ 2\sum_{i=1}^m N_{I,\beta}(\mathbf{u}_i) N_{I',\beta'}(\mathbf{u}_i)\ \ldots \\ \vdots \end{pmatrix},$$

$$\mathbf{c} = (\ldots, -2\sum_{i=1}^{m} \mathbf{p}_i N_\beta^I(\mathbf{u}_i), \ldots)^T,$$

and $f = \sum_{i=1}^m \|\mathbf{p}_i\|^2$.

The fairness functional E_{fair} is also a quadratic function in the unknown control points, and can be written in a similar fashion. However, the computation of the fairness functional is usually time-consuming since it requires the integration over a product of two splines. Similar to [10], we do not use the traditional fairness functional, which requires integration of products of spherical splines. Instead, we employ a set of linear constraints on the control points.

Let $[\mathbf{t}_{0,\beta_0}, \mathbf{t}_{1,\beta_1}]$ be an edge of the spherical triangulation. Denote $I = (\mathbf{t}_0, \mathbf{t}_1, \mathbf{t}_2)$ and $J = (\mathbf{t}_0, \mathbf{t}_1, \mathbf{t}_3)$ its two adjacent triangles. Let $\mathbf{F}^I = \sum_{|\beta|=n} \mathbf{c}_{I,\beta} N(\mathbf{u}|V_\beta^I)$ be the polynomial on triangle I and similarly for $\mathbf{F}^J$. Let f^I and f^J be the polar forms of $\mathbf{F}^I$ and $\mathbf{F}^J$, respectively. Then, we require

$$\mathbf{c}_{I,\beta} = f^J(X_\beta^I), \forall \beta, |\beta| = n, \beta_2 \le r \tag{3}$$

where $0 \le r \le n-1$ is an integer ($r = 2$ and $n \ge 5$ in our implementation) which controls the fairness of the spline surface. Equation (3) is a linear equation of the control points.

We refer the readers to [11, 12, 10] for the detailed information about the polar form and fairing triangular *B*-spline surfaces.

Therefore, the above optimization problem can be stated as follows:

$$\begin{aligned} \min \quad & \frac{1}{2}\mathbf{x}^T Q\mathbf{x} + \mathbf{c}^T\mathbf{x} + f \\ \text{subject to} \quad & A\mathbf{x} = \mathbf{b}, \end{aligned} \tag{4}$$

which is a typical constrained convex quadratic programming problem, and can be solved by the interior-point based method efficiently.

Algorithm 1: automatic conversion brain surface to spherical spline
Input: brain surface M with m points, $\{\mathbf{p}_i\}_{i=1}^m$*, degree n, maximal fitting tolerance* ε*, number of triangles N in the initial spherical domain.*
Output: a degree n spherical triangular B-spline $\mathbf{F}$ *which approximates M.*

1. *Calculate the spherical conformal parameterization of M using Gu et al. method [3]. Denote by* $h : M \to \mathbb{S}^2$ *this conformal map, i.e.,* $h(\mathbf{p}_i) = \mathbf{u}_i \in \mathbb{S}^2$.
2. *Decimate M to a simplified mesh* $\tilde{M}$ *with N triangles. Map* $\tilde{M}$ *to the sphere. Construct an initial spherical triangular B-spline of degree n based on the spherical triangulation of* $\tilde{M}$.
3. *Solve Equation (4) by considering control points as free variables.*
4. *Check the maximal fitting error for each spherical triangle* Δ_I*. If it violates the criterion, i.e.,* $\max_{\mathbf{u}_i \in \Delta_I} \|\mathbf{F}(\mathbf{u}_i) - \mathbf{p}_i\| > \varepsilon$*, subdivide the triangle* Δ_I *using 1-to-4 scheme and then split the neighboring triangles to avoid T-junctions.*
5. *If the maximal fitting error on each triangle satisfies the user-specified fitting tolerance* ε*, exit; Otherwise, go to step 3.*

3 Brain Surface Analysis

By converting dense meshes/point clouds to spherical splines, we achieve a compact and highly continuous representation. More importantly, we have the analytical form of the underlying shape. Thus, we can compute the normals, curvatures, geodesics, areas, etc., anywhere on the surface. These differential properties are crucial in the brain image analysis. In this section we demonstrate the efficacy of analyzing the brain surface using spherical splines.

3.1 Segmentation by the mean curvature

The computation of curvature is essential in shape analysis, segmentation and registration. There are many techniques to estimate the curvature on polygonal meshes, e.g., [13–18]. These methods use either discrete differential operators or local polynomial fitting to approximate the curvature tensor. Therefore, the estimation results closely rely on the connectivity and quality of the input meshes.

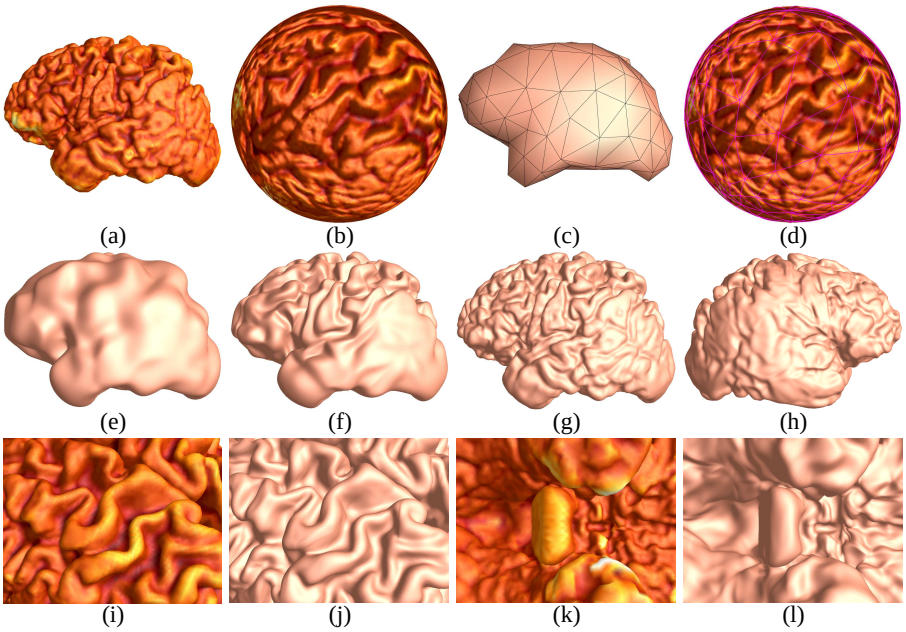

Fig. 2. Illustration of surface reconstruction using spherical splines. The input is a triangular mesh M with $131K$ triangles (a). We first compute its conformal spherical parameterization shown in (b). Then we simplify the mesh to 280 triangles (shown in (c)) and map it to the sphere as the initial spherical domain (shown in (d)). From (e) to (g), we fit the mesh M using a degree 5 spherical spline with 280, 1048 and 2086 spherical triangles. The root-mean-square error (r.m.s.) are 0.328%, 0.0951%, 0.0196% of the diagonal of the input mesh, respectively. (h) shows the back view of the reconstructed spline. (i) and (k) show the closeup of the original mesh. (j) and (l) show the closeup of the reconstructed spline. Note that the high continuity (C^4-continuous) of our spline surface.

In our framework, we convert the brain surface into a single spherical spline of high continuity. Thus, the Gaussian curvature K and mean curvature H can be computed analytically and efficiently without resorting to any numerical approximations.

Curvature features such as zero contours and maxima are useful for surface matching and object recognition. After computing the curvature values, we can easily locate the curvature zero contours, which are helpful for segmenting the brain surface into regions (the gyri and the sulci).

3.2 Tracing the sulci and gyri lines

The major sulci and gyri on the cortical surface have distinct geometric properties and are conserved between individuals, making them useful landmarks for morphometric comparisons. From computer vision's point of view, these sulci and gyri are closely related to the ridge-valley lines, which are curves on a surface along which the surface bends sharply. The ridge-valley lines are powerful shape descriptors that provides us

with important information about the shapes of objects. Therefore, robust extraction of ridge-valley structures is important for brain image analysis.

In [19], Belyaev et al. present a mathematical description of such surface creases by the extrema of the principal curvatures along their curvature lines. For a spherical spline surface $\mathbf{F}(u,v)$, denote by $k_{max}(u,v)$ and $k_{min}(u,v)$ the maximal and minimal principal curvatures, $k_{max} \geq k_{min}$. Let $\mathbf{t}_{max}(u,v)$ and $\mathbf{t}_{min}(u,v)$ be the corresponding principal directions. Consider the derivatives of the principal curvatures along their corresponding directions $e_{max}(u,v) = \partial k_{max}/\partial \mathbf{t}_{max}$ and $e_{min}(u,v) = \partial k_{min}/\partial \mathbf{t}_{min}$. The extrema of the principal curvatures along their curvature directions are given by the zero-crossings of e_{max} and e_{min}, and the ridges and valleys are characterized by

$$e_{max} = 0, \partial e_{max}/\partial \mathbf{t}_{max} < 0, k_{max} > |k_{min}|, (ridges), \tag{5}$$

$$e_{min} = 0, \partial e_{min}/\partial \mathbf{t}_{min} > 0, k_{min} < -|k_{max}|, (valleys). \tag{6}$$

Note that if we change the surface orientation, then the ridges turn into the ravines and vice versa.

Similar to [20], we measure the strength of a ridge line by the integral of k_{max} along the line, i.e., $\int k_{max} ds$. The ridges whose strength are less than the user-specified threshold are ignored.

Algorithm 2: automatic tracing the sulci and gyri lines
Input: a spherical spline $\mathbf{F}$*, N resolution of the output mesh,* λ_{thres}
Output: a set of ridge (gyri) curves and a set of valley (sulci) curves.

1. *Evaluate the spline* $\mathbf{F}$ *and get the mesh* M_s *containing N triangles.*
2. *For each vertex* $\mathbf{v} \in M_s$*, compute* e_{max} *and* e_{min}*. Mark* $\mathbf{v}$ *as feature point if it satisfies Equation (5) and (6).*
3. *For each edge* $(\mathbf{v}_i, \mathbf{v}_j) \in M_s$*, let* $h(\mathbf{v}_i) \in \mathbb{S}^2$ *and* $h(\mathbf{v}_j) \in \mathbb{S}^2$ *be the spherical parameters of vertex* $\mathbf{v}_i$ *and* $\mathbf{v}_j$ *respectively. If* $e(h(\mathbf{v}_i))e(h(\mathbf{v}_j)) < 0$*, perform the 1-D search on the edge to get the vertex* $\tilde{\mathbf{v}} \in (\mathbf{v}_i, \mathbf{v}_j)$ *such that* $e(h(\tilde{\mathbf{v}})) = 0$*. Mark* $\tilde{\mathbf{v}}$ *as feature point.*
4. *Trace the feature points to get feature curves.*
5. *Compute the strength* $T = \int k_{max} ds$ *of each feature curve. Output the curve if* $T \geq \lambda_{thres}$*.*

The output of Algorithm 2 usually contains large number of sulci and gyri. Sometimes, the doctors are interested only in part of them. For example, seven major sulci are used in [6]. Our system allows the user to interactively select the desired sulci from the output of Algorithm 2. We also provide the functionality to automatically connect two user-specified sulci.

3.3 3D Shape comparison using conformal representation

In [4], Gu and Vemuri present a systematic method for 3D shape comparison using conformal representations. By stereographic projection, the unit sphere (except the north pole) can be mapped to the (u,v) plane, the mapping can be represented as

$$(x,y,z) \rightarrow (u,v) : (u,v) = \frac{1}{1-z}(x,y).$$

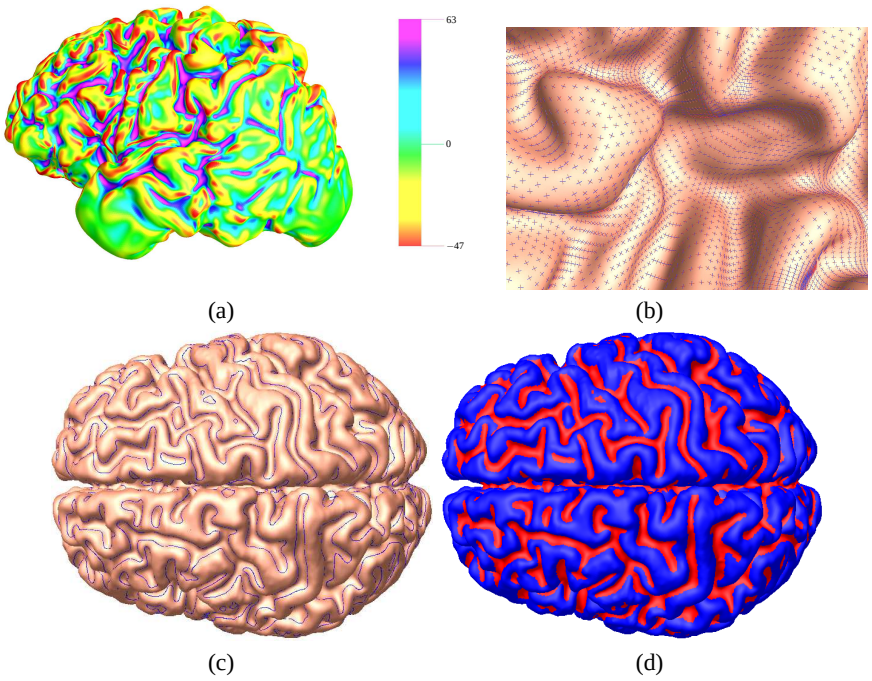

Fig. 3. Computing the curvature on the cortical surface: (a) Mean curvature; (b) Close-up of the principal directions; (c) The zero contour of the mean curvature; (d) Segmentation of gyri and sulci by the sign of mean curvature.

The metric (first fundamental form) of the sphere is represented as

$$ds_0^2 = \frac{4(du^2+dv^2)}{(1+u^2+v^2)^2}.$$

Any closed genus zero surface Σ can be mapped to the unit sphere by a diffeomorphism $\phi : \Sigma \to S^2$. Therefore, (u,v) is also a local parameter coordinate system of Σ, such that the metric of Σ can be represented as

$$ds_\Sigma^2 = \lambda(u,v)ds_0^2, \lambda(u,v) \in \mathbb{R}^+.$$

It can be demonstrated that ϕ preserves the angles; namely, any two intersecting curves on Σ will be mapped to two curves on S^2 such that the intersecting angle is preserved. These kinds of mappings are called *conformal* maps, and $\lambda(u,v)$ is called the *conformal factor*. There are infinite conformal maps from Σ to S^2. Assume $\phi_i : \Sigma \to S^2, i = 0,1$ are two conformal maps, then their difference $\phi_1 \circ \phi_0 : S^2 \to S^2$ is a *Möbius* transformation. In (u,v) coordinates, it has the form

$$\frac{az+b}{cz+d}, z = u+iv, a,b,c,d \in \mathbb{C}, ad-bc = 1.$$

Gu and Vemuri demonstrated that Σ can be determined by the conformal factor $\lambda(u,v)$ and its mean curvature $H(u,v)$ uniquely up to rigid motion in $\mathbb{R}^3$. Therefore, (λ,H) under the conformal parameterization (u,v) is the *conformal representation* of the surface Σ.

In order to compare shape Σ_1 and Σ_2, it is sufficient to measure the distance between their conformal representations. Suppose (λ_1,H_1) and (λ_2,H_2) are the conformal representations of Σ_1 and Σ_2 respectively; the distance between them is formulated as

$$E(\Sigma_1,\Sigma_2) = \inf_{\tau} \int_{S^2} (\lambda_1 - \lambda_2 \circ \tau)^2 + (H_1 - H_2 \circ \tau)^2 ds, \tau \in \textit{Mobius Group} \qquad (7)$$

In [4], the conformal factor is approximated using a piecewise linear function, and mean curvature is approximated by the discrete Laplace-Beltrai operator. The approximation is brute force and inaccurate.

In our current implementation, we represent the brain surfaces using C^4 smooth splines with the user specified tolerance. Since we use spherical conformal parametrization to construct the spherical spline, the computation of the conformal factor and mean curvature are direct and without any approximation.

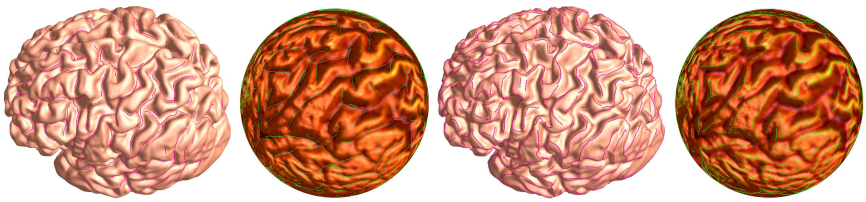

(a) (b) (c) (d)

Fig. 4. Automatic tracing the sulci and gyri: (a) Sulci (cyan curves) on the brain surface; (b) Sulci (green curves) on the spherical domain; (c) Gyri (cyan curves) on the brain surface; (d) Sulci (green curves) on the spherical domain. The number of detected sulci and gyri are 412 and 528, respectively.

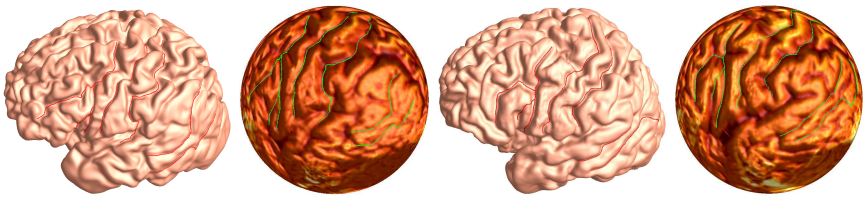

(a) (b) (c) (d)

Fig. 5. Illustration of seven major sulci of the left brain hemisphere of two different brain surfaces. Only few user interactions are needed to specify the desired sulci.

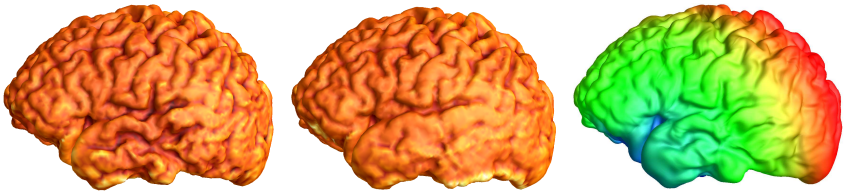

(a) Brain surface A (b) Brain surface B (c) Displacement field

Fig. 6. 3D shape comparison using conformal representation. (a) and (b) show two brain surfaces. The displacement field is color-encoded as shown in (c).

4 Experimental results

We have implemented a prototype system on a 3GHz Pentium IV PC with 1GB RAM. We perform experiments on two brain surfaces (shown in Figure 6(a) and (b)) which are obtained from 3D $256 \times 256 \times 124$ T1 weighted SPGR (spoiled gradient) MRI images, by using an active surface algorithm that deforms a triangulated mesh onto the brain surface [21]. In order to compare the fitting qualities for different test cases, we uniformly scale the data into a unit cube.

Table 1. Statistics of the surface approximation algorithm. Mesh size: M_v, # of vertices, M_f, # of faces; Spline configuration: n, degree of spherical splines, N_t, # of domain triangles, N_c, # of control points, *r.m.s.*, root mean square error, L_∞, maximal error.

Subject	M_v	M_f	n	N_t	N_c	*r.m.s.*	L_∞
A	65,538	131,072	5	2,086	26,077	0.0196%	0.155%
B	65,538	131,072	5	2,012	25,152	0.0201%	0.176%

We first convert these brain images into spherical triangular *B*-spline representation by Algorithm 1. In order to compute the ridge and valley curves accurately, we need to compute the fourth order derivative of the spline surface. Therefore, in our experiments, we use degree 5 spherical splines which are C^4-continuous everywhere. The fitting procedure takes about 30 to 40 minutes for each test case. Figure 2 illustrates the pipeline of our surface reconstruction algorithm on test case A. Table 1 shows the input mesh size, spline configuration and fitting quality. Compared to the discrete mesh representation, our spherical spline based representations have low storage requirements and can achieve high accuracy (e.g., root-mean-square error $\leq 0.02\%$) as well as high continuity (C^4).

Figure 3 shows the computation of mean curvature, principal directions, and the zero-crossing of the mean curvature of the reconstructed brain surface A.

Figure 4 shows the detected sulci and gyri on the reconstructed brain surface A and its spherical domain. The number of detected sulci and ridges for are 412 and 528 respectively. The time for tracing feature curves is less than 1 minute for both test cases. Figure 5 shows seven major sulci of the left brain hemisphere of two different brain surfaces. These sulci are selected by the users with only very few interactions.

Figure 6 shows the results of 3D shape comparison using conformal representation. The conformal factor $\lambda(u,v)$ and mean curvature $H(u,v)$ are computed analytically using spherical splines.

5 Conclusion

In this paper, we propose a spherical spline based framework for brain surface analysis. We present automatic algorithm to convert a brain mesh into a spherical triangular *B*-spline whose maximal error deviation from the original data is less than the user-specified tolerance. With the analytical representation of the brain model, we can easily compute various differential properties, such as conformal factor, mean curvature, principal directions, geodesics, etc, accurately and robustly. By studying the extrema of the principal curvatures with respect to the curvature directions, we present an automatic algorithm to trace the gyri and sulci. Furthermore, we can solve the 3D shape comparison using conformal representation directly without resorting to any numerical approximation. Experimental results show the efficacy of using spherical splines in brain image analysis.

References

1. Avants, B.B., Gee, J.C.: The shape operator for differential analysis of images. In: IPMI. (2003) 101–113
2. Cachia, A., Mangin, J.F., Rivière, D., Boddaert, N., Andrade, A., Kherif, F., Sonigo, P., Papadopoulos-Orfanos, D., Zilbovicius, M., Poline, J.B., Bloch, I., Brunelle, F., Régis, J.: A mean curvature based primal sketch to study the cortical folding process from antenatal to adult brain. In: MICCAI. (2001) 897–904
3. Gu, X., Wang, Y., Chan, T.F., Thompson, P.M., Yau, S.T.: Genus zero surface conformal mapping and its application to brain surface mapping. In: IPMI. (2003) 172–184
4. Gu, X., Vemuri, B.C.: Matching 3d shapes using 2d conformal representations. In: MICCAI (1). (2004) 771–780
5. Tao, X., Han, X., Rettmann, M.E., Prince, J.L., Davatzikos, C.: Statistical study on cortical sulci of human brains. In: IPMI. (2001) 475–487
6. Tao, X., Prince, J.L., Davatzikos, C.: An automated method for finding curves of sulcal fundi on human cortical surfaces. In: ISBI. (2004) 1271–1274
7. Thompson, P.M., Toga, A.W.: A surface-based technique for warping 3-dimensional images of the brain. IEEE Trans. Medical Images **15** (1996) 402–417
8. Thompson, P.M., Mega, M.S., Vidal, C., Rapoport, J.L., Toga, A.W.: Detecting disease-specific patterns of brain structure using cortical pattern matching and a population-based probabilistic brain atlas. In: IPMI. (2001) 488–501
9. Pfeifle, R., Seidel, H.P.: Spherical triangular b-splines with application to data fitting. Comput. Graph. Forum **14** (1995) 89–96
10. He, Y., Gu, X., Qin, H.: Fairing triangular *B*-splines of arbitrary topology. In: Proceedings of Pacific Graphics '05. (2005) to appear
11. Seidel, H.P.: Polar forms and triangular *B*-spline surfaces. In Du, D.Z., Hwang, F., eds.: Euclidean Geometry and Computers, 2nd Edition. World Scientific Publishing Co. (1994) 235–286

12. Gormaz, R.: *B*-spline knot-line elimination and Bézier continuity conditions. In: Curves and surfaces in geometric design. A K Peters, Wellesley, MA (1994) 209–216
13. Meyer, M., Desbrun, M., Schröder, P., Barr, A.H.: Discrete differential-geometry operators for triangulated 2-manifolds. In: VisMath '02. (2002)
14. Taubin, G.: Estimating the tensor of curvature of a surface from a polyhedral approximation. In: ICCV. (1995) 902–907
15. Goldfeather, J., Interrante, V.: A novel cubic-order algorithm for approximating principal direction vectors. ACM Trans. Graph. **23** (2004) 45–63
16. Rusinkiewicz, S.: Estimating curvatures and their derivatives on triangle meshes. In: 3DPVT. (2004) 486–493
17. Surazhsky, T., Magid, E., Soldea, O., Elber, G., Rivlin, E.: A comparison of gaussian and mean curvatures estimation methods on triangular meshes. In: ICRA. (2003) 1021–1026
18. Theisel, H., Rössl, C., Zayer, R., Seidel, H.P.: Normal based estimation of the curvature tensor for triangular meshes. In: Pacific Conference on Computer Graphics and Applications. (2004) 288–297
19. Belyaev, A.G., Pasko, A.A., Kunii, T.L.: Ridges and ravines on implicit surfaces. In: Computer Graphics International. (1998) 530–535
20. Ohtake, Y., Belyaev, A.G., Seidel, H.P.: Ridge-valley lines on meshes via implicit surface fitting. ACM Trans. Graph. **23** (2004) 609–612
21. Thompson, P.M., Toga, A.W.: A framework for computational anatomy. Computing and Visualization in Science **5** (2002) 1–12